PVT AND FLOW BEHAVIOR OF IMPURE CO_2 IN AQUIFERS

O. Sævareid[1*], S.E. Gasda[1], T.S. Mykkeltvedt[1]

[1] NORCE, Bergen, Norway

* Corresponding author e-mail: ovsa@norceresearch.no

Abstract

We combine compositional modelling of a Brine-CO_2 system with detailed resolution of the well interface and the near-well reservoir region. Via a small selection of case studies, we explore how impurities added to a CO_2 injection stream impacts reservoir flow and well response.

Keywords: *CO_2 injection, Impurities, Density, Viscosity, Well-Reservoir*

1. Introduction

The planning and control of CO_2 injection operations depends crucially on accurate and efficient simulation tools. Uncertainty regarding reservoir description, temperature conditions and the amount and type of impurities inherent in the CO_2 stream, are some of the aspects that must be explored.

This paper considers the near-well reservoir under injection, and address sensitivity of mixture properties in interaction with some simple reservoir structures. Towards this end, first we apply an in-house PVT tool [1] to explore some basic properties of impure CO_2 mixtures. For reservoir flow we have used a model available via the OPM framework [13]. This is a compositional model for a CO2-Brine system based on a nonlinear complementary formulation[4][9]. The model relies on [5][15][16] for mutual dissolution between CO_2 and brine. Density and viscosity for the liquid (H2O-rich) phase are based on [2][3][8], while the properties for the "gas" (CO2-rich) phase are modelled according to [6][14][17].

2. Sensitivity of mixture PVT properties

Our focus here will be sensitivity of density and viscosity of the CO_2-rich phase with respect to impurities.

We consider a mixture of about 50% mole fraction water, while the remaining fraction consists of CO_2 where "impurities" are added by replacing 5-10% of the CO_2 by combinations of N_2 and CH_4.

We base our study on an in-house PVT tool using the Peng-Robinson equation of state and use the group contribution method, see [12] and references therein, to compute binary interaction parameters (BIP).

Table 1: Temperature dependent binary interaction coefficients computed by group contribution method for two different temperatures. Below diagonal coefficients for T=293K and above diagonal coefficients for T=353K.

	H_2O	N_2	CO_2	CH_4
H_2O		0.5453	-0.0735	0.4485
N_2	0.7826		-0.0811	0.0456
CO_2	-0.1039	-0.0554		0.1230
CH_4	0.5873	0.0424	0.1098	

For a set of alternative interaction parameters, we have also collected coefficients from the online calculator at *https://checalc.com/solved/multi_flash.html*. These are partially based on correlations given by Gao et.al [7], and coefficients obtained for our fluid system are shown in Table 2 below.

Table 2: Alternative binary interaction coefficients.

	H_2O	N_2	CO_2	CH_4
H_2O				
N_2	0.0753			
CO_2	0.1200	-0.0170		
CH_4	0.0444	0.0311	0.0919	

Variability across choices of interaction parameters, is clearly significant, but the sensitivities regarding impurities are of similar magnitude.

2.1 Density

Densities for the CO_2-rich phase obtained from various mixtures and based on the parameters from Table 2, are depicted in Figure 1 and Figure 2 for temperatures of 293K and 353K, respectively.

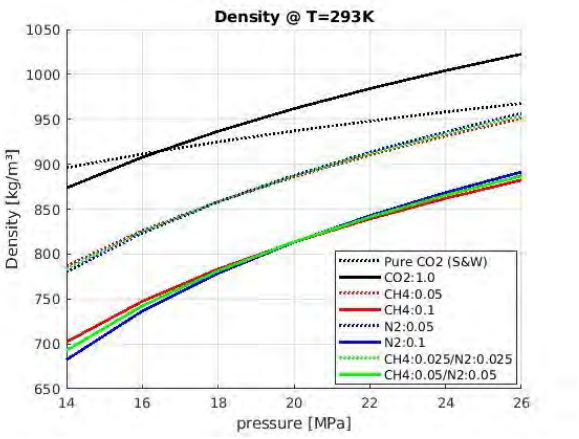

Figure 1: Density for CO2-rich phase at "low" temperature.

The mole fractions shown in the curve legends refer to the feeding gas mixture, i.e., before brought into equilibrium with an abundant water-rich phase. Thus, the solid black line refers to the CO_2-rich phase of CO_2-H_2O system. For comparison, the density of pure CO_2 is shown as dotted black lines, based on Span& Wagner [14]. The colored lines represent various impure feeding gas mixtures, while solid and dotted indicates 90% respectively 95% mole fraction of CO_2. Red lines represent impurities in terms of methane, blue is nitrogen, and green is an equal weight (mole fraction) combination of the two.

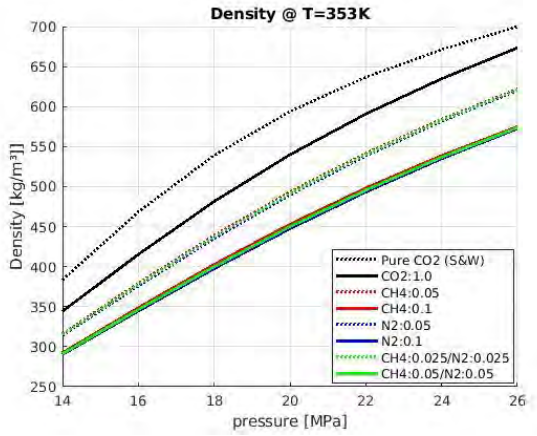

Figure 2**:** Density for CO_2-rich phase at "high" temperature.

The model shows clear sensitivity for the magnitude of impurity, while the quality appears to be much less important for the substances and compositions considered here. For pressure 22MPa and temperature 353K we observe densities for impure mixtures at approximately 80% and 90% of that of the pure CO_2-water system. For temperature 293K, the relative impact is slightly less.

2.2 Viscosity

Viscosities are calculated using both the original and improved LBC models, refer [10][11]. The two models give essentially identical output for the CO_2-rich phase, and results for temperatures 293K and 353K are shown in Figure 3 and Figure 4 below. The organization of line types and legends correspond to the above density plots.

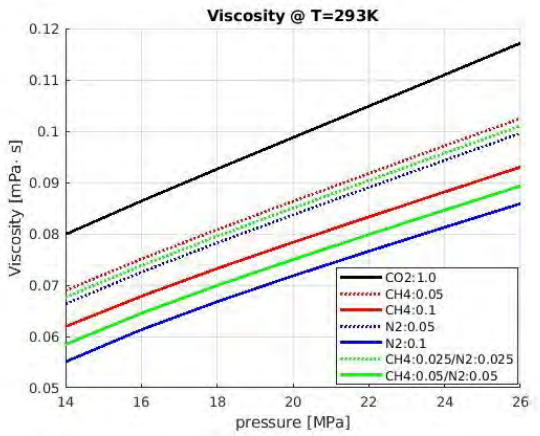

Figure 3: Viscosity for "cold" CO_2 mixtures.

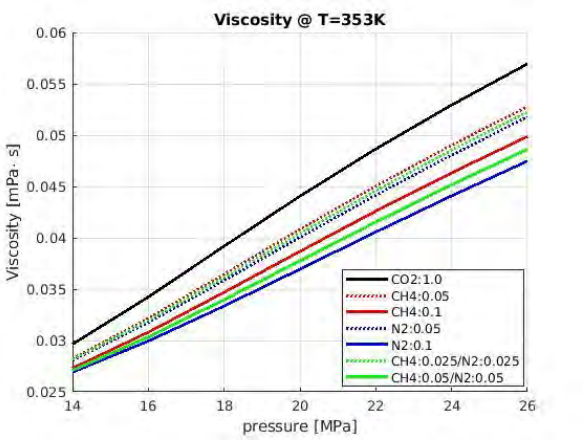

Figure 4: Viscosity for "hot" CO_2 mixtures.

Compared to the density results where the magnitude of the impurities was the dominating factor, we note that the viscosities display a clear sensitivity also regarding the quality of the impurities. For pressure 22MPa and temperature 293K we observe viscosities for the equal weighted impurities (green lines) approximately 75% and 85% of that of the pure CO_2-water system. For temperature 353K, the relative impact is less.

A more complete view of the viscosities is shown in Figure 5 and Figure 6 below, corresponding to mixtures of 90% and 95% mole fraction CO_2, respectively.

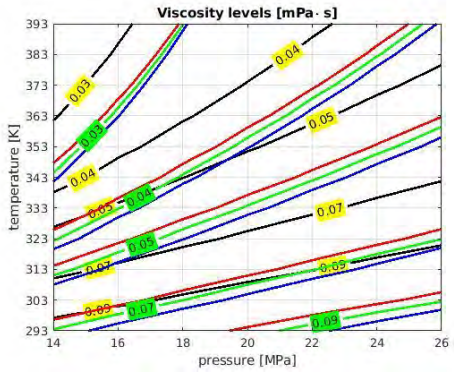

Figure 5: Viscosity contours for 90% CO_2 mole fraction.

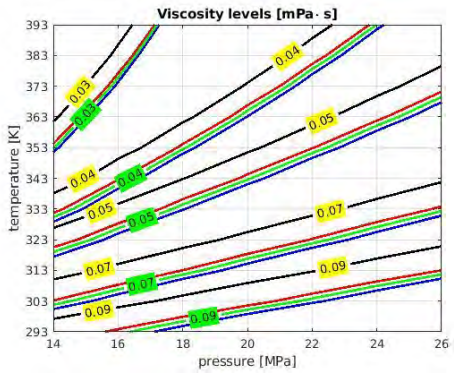

Figure 6: Viscosity contours for 95% CO_2 mole fraction.

The above computations verify the common knowledge that adding relevant impurities to a CO_2 stream, typically decrease both density and viscosity. From an injection perspective, these changes will partly cancel each other. Lower densities require more volume injected to deposit the same mass, while smaller viscosity will promote flow. Added chemical complexity increases risk for permeability altering precipitation. From a storage perspective, the plume will be larger, more buoyant, and presumably less leakage resistant.

3. Impact on reservoir flow

Here, we will first establish a simple reservoir model and then apply it to investigate how basic properties of the injected CO_2 stream influence the flow behavior in the reservoir. Model geometry is outlined in Figure 7 below, and some basic quantities are listed in Table 3.

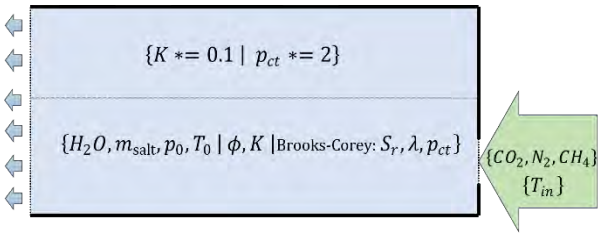

Figure 7: Computational domain for flow sensitivity study.

We consider an annular sector extending from an inner radius of 0.1m, aiming for a direct representation of the well-reservoir interface. The reservoir has a height of 40m, and the well is completed for inflow between 5m and 15m from the bottom as indicated along the right edge in Figure 7. Flow is specified in terms of uniformly distributed mass rates. The radial extent used for the computations shown here is 90m. Top and bottom boundaries are closed, while the outer radius is open for flow. Initially the reservoir is filled with water where small amounts of salt and CO_2 are dissolved. The fluid is in hydrostatic equilibrium (datum 250MPa at reservoir bottom) and at uniform temperature T_0=353K. The reservoir is partitioned into two layers, confer the horizontal dotted line in Figure 7, where the upper region (18m) is assumed to have a more fine-grained structure, more adverse to CO_2 intrusion.

Table 3 Reservoir and flow characteristics for the lower, coarse grained part of the reservoir. The upper, fine grained material has one-tenth the K and twice the p_{ct}.

Property	Value
Permeability (K)	1 Darcy
Porosity (Φ)	0.3
Brooks-Corey parameter (λ)	2.0
Capillary threshold pressure (p_{ct})	5000 Pa
Residual brine saturation	0.2
Residual CO_2 saturation	0.0

3.1 Base case

Our baseline injection stream corresponds to pure CO_2, and the temperature T_{in}=353K equals the initial reservoir temperature T_0. The injection rate is set to approximately 170000 Sm^3/day. Selected snapshots of the developing flow are depicted in Figure 8.

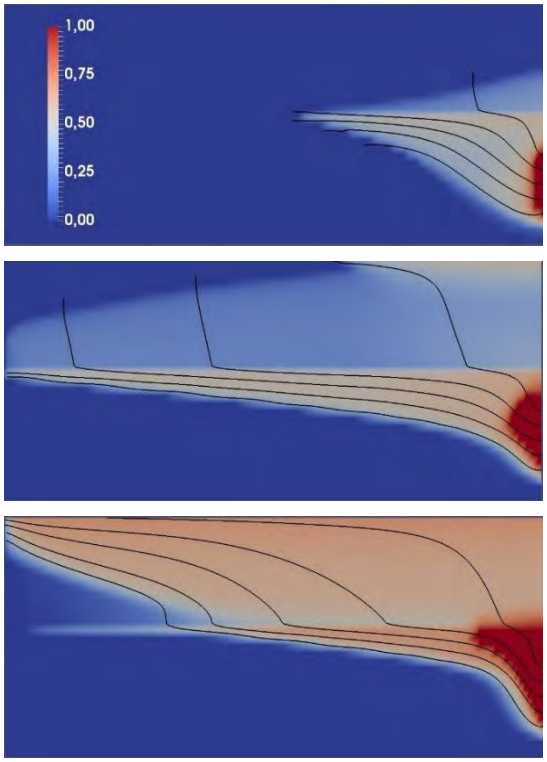

Figure 8 Saturation and streamlines for the CO_2-rich phase. Base case behavior at day 10, 100 and 1000, respectively.

Initially the bulk of the injection stream is confined below the material interface, fingering through the brine, and establishing a channel connecting to the outflow boundary. Gradually the buoyancy overcomes the vertical obstacle, and a continuous phase is formed also in the upper, fine-grained material, allowing the CO_2-rich phase an alternative escape route. This self-reinforcing process eventually erodes the original channel through the coarse-grained sand, and in the end, the whole injection stream is directed upwards. From Figure 9 we conclude that in terms of CO_2 retained, a steady state is reached after slightly more than one year of injection for our baseline scenario.

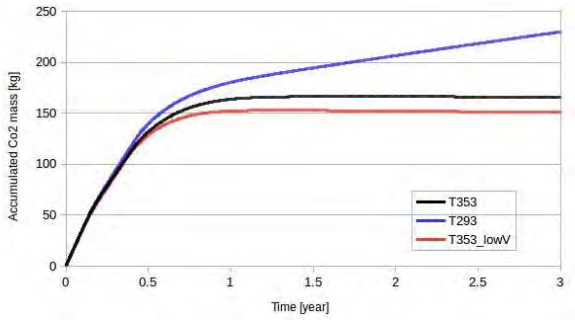

Figure 9 CO_2 mass retained in the reservoir. Base case (black), low viscosity (red), and cold (blue).

The scenario outlined in Figure 8 is observed for all parameter combinations considered in this study. However, we have essentially confined ourselves to explore the impact of varying viscosity and temperature for the injection mixture. Extending the scope to also include e.g., the parameters of Table 3, might reveal different behavior.

From Figure 8, we observe that the brine phase disappears in the vicinity of the well. With a residual saturation of 0.2, this indicates that the brine originally present has evaporated into the CO_2-rich phase. The associated salt precipitation causing permeability alterations is a well-known reason for injectivity problems. We will not pursue this aspect further here but note that our simulations easily can be adapted to include this effect.

3.2 Low viscosity injection mixture

We mimic an impure CO_2 injection stream by reducing the viscosity to 80% compared to base case, confer the discussion in section 2.2 above. Injection rate and temperature are kept as for the base case.

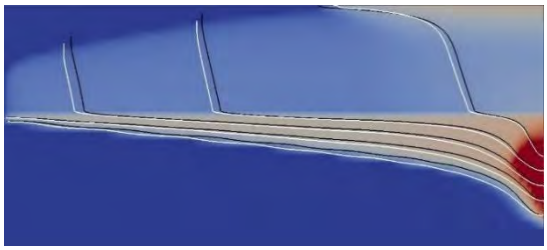

Figure 10 Saturation and streamlines for CO_2-phase. Low viscosity injection mixture at 100 days. White streamlines show base case behavior.

Compared to the base case, Figure 10 indicates a slightly leaner channel that penetrates at a higher speed through the brine to reach the outflow boundary. Also, the migration of the CO_2-rich phase into the upper, fine-grained region, as well as the erosion of the primary channel, are faster. That the less viscous mixture also displaces less brine and thus leads to less CO_2 retained, confer Figure 9, is also to be expected.

3.3 Cold injection mixture

We here lower the injection temperature. Setting T_{in}=293K yields a contrast of 60K compared to the initial reservoir temperature T_0. Our calculations from section 2 indicates typically 50% increased density and viscosity for the CO_2-rich phase.

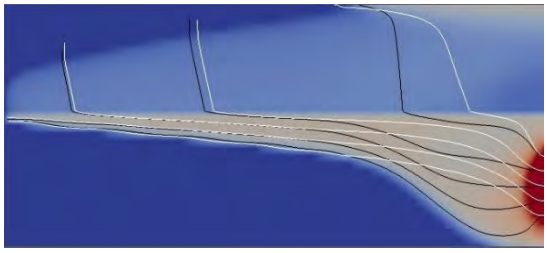

Figure 11 Saturation and streamlines for CO_2-phase. Cold injection mixture at 100 days. White streamlines are corresponding base case behavior.

We see from Figure 11 that after 100 days of injection the difference versus the base case is most pronounced in the vicinity of the well. Here the effect of the cold injection stream is more immediate, and the reservoir volume to be influenced is relatively small.

From Figure 9, we also note that for the cold injection stream, the amount of CO_2 retained increases steadily for the hole injection period. This effect must be attributed to a continuous cooling of the reservoir, leading to a gradually denser and more viscous CO_2-rich phase providing more efficient displacement and storage capabilities.

3.4 Injection well

The pressures (CO_2-rich phase) depicted in Figure 12, are the difference between the flowing pressure at the well-reservoir interface and the initial hydrostatic pressure. They are all sampled at the midpoint of the open well segment, located 10m from the reservoir bottom, corresponding to the origin of the central streamline. The absolute size of the pressure buildup obviously depends on the injection rate and for low to moderate rates it can be supposed to scale linearly with the rate. Thus, the sensitivities indicated by Figure 12 and Figure 13 can be extrapolated with some degree of confidence.

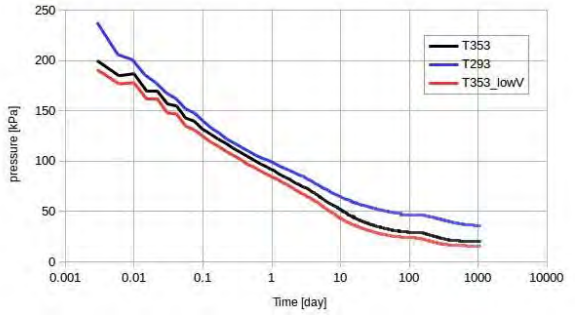

Figure 12 Well pressure buildup. Logarithmic time axis to show the early transient period. Base case (black), low viscosity (red), and cold (blue).

Figure 13 depicts the pressure along the radial (horizontal) direction extending from the well interface into the reservoir (time=100 in Figure 12 corresponds to radius=0.1 in Figure 13). The locations of transition to single phase brine regions are evident.

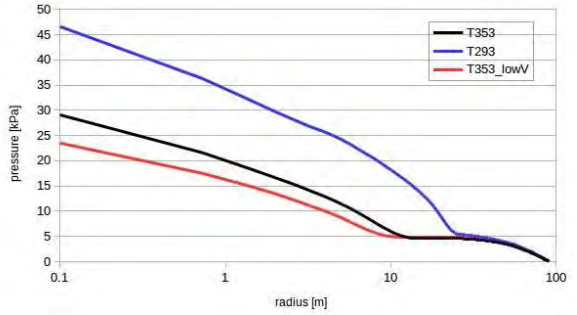

Figure 13 Radial pressure along well centerline at 100 days. Logarithmic radial axis to detail the near well behavior. Base case (black), low viscosity (red), and cold (blue).

Our approach aims at a direct resolution of the well reservoir interface. Depending on the application, various measures can be applied to improve the computational accuracy. The wiggles observed in Figure 12 for the first hours indicates a potential for more careful control of the time stepping. The discrete spatial resolution, currently ~0.5m in the well vicinity, can likewise be modified. If the early transients are important, gradually ramping up the injection rate is operationally realistic and promotes numerical stability.

4. Conclusion

Focusing on the well-reservoir interface and the near-well region, we have performed sensitivity studies on the effects of impurities and temperature variations in CO_2 injection streams.

A more systematic exploration of the parameter space remains, regarding both PVT behavior and rock properties. However, we believe that our preliminary results shed some light on the variability of accumulation and well response due to changing properties of the injection stream.

Combining geometrical resolution and detailed compositional fluid modelling has potential use as a detailed planning or control tool for well operations. Another application will be calibration and verification of simplified pseudo models for integration in large scale field simulations.

Depending on application and required level of completeness, our approach might benefit from the inclusion of a detailed wellbore model that can interact directly with the reservoir model via mutual boundary conditions at the well interface.

The current reservoir model is originally a Brine-CO_2 compositional model where we have manipulated high level properties (density/viscosity) to mimic impact of impurities. For exploration of more subtle effects like mutual dissolution or precipitation, more fine-grained control can be added.

Acknowledgements

This publication has been produced with support from research program CLIMIT and the NCCS Research Centre, performed under the Norwegian research program Centres for Environment-friendly Energy Research (FME) and the Research Council of Norway (257579/E20 and 280394).

References

[1] Aavatsmark, I., Kometa, B.K., Gasda, S.E., Sandve, T.H. & Nilsen, H.M. (2016). A generalized cubic equation of state with application to pure CO2 injection in aquifers. Comput Geosci 20, 623–635

[2] Adams, J. and Bachu, S., 2002, Eq. of state for basin geofluids: algorithm review and intercomparison for brines, Alberta Geological Survey, Edmonton, Canada.

[3] Batzle, M. and Wang, Z., 1992, Seismic properties of pore fluids, Geophysics, Vol. 57, No. 11, 1396 – 1408.

[4] Bui, Q.M. & Elman, H.C. (2020). "Semi-smooth Newton methods for nonlinear complementarity formulation of compositional two-phase flow in porous media." Journal of Comp. Physics, 407, 109163

[5] Duan, Z., Sun, R., 2003. An improved model calculating CO2 solubility in pure water and aqueous NaCl solutions from 257 to 533 K and from 0 to 2000 bar. Chemical Geology 193, 257–271.

[6] Fenghour, A., Wakeham, W., and Vesovic, V.. (1998). The Viscosity of Carbon Dioxide. Journal of Physical and Chemical Reference. 27:31-44

[7] Gao, G., Daridon, J.-L., Saint-Guirons, H. Xans, P. & Montel, F. (1992). "A simple correlation to evaluate binary interaction parameters of the Peng-Robinson equation of state: binary light hydrocarbon systems." Fluid Phase EquilibriaVolume 74, 85-93.

[8] Garcia, J. (2001) "Density of Aqueous Solutions of CO2". Tech Report, LBNL Report 49023; Lawrence Berkeley National Laboratory: Berkeley, CA, USA.

[9] Lauser, A., Hager, C., Helmig, R. & Wohlmuth B. (2011) "A new approach for phase transitions in miscible multi-phase flow in porous media" Adv. Water Resour., 38, 957-966

[10] Lansangan, R.M., Taylor, M., Smith, J.L. and Kovarik, F.S. (1993). "An improved viscosity correlation for CO2 / reservoir oil systems." SPE Advanced Technology Series, 1(2), 134–141.

[11] Lohrenz, J., Bray, B.G. and Clark, C.R. (1964) "Calculating viscosities of reservoir fluids from their composition." Journal of Petroleum Technology, 16(10), 1171–1176.

[12] Qian, J.W., Privat, R. & Jaubert, J.N. (2013). Predicting the Phase Equilibria, Critical Phenomena, and Mixing Enthalpies of Binary Aqueous Systems Containing Alkanes, Cycloalkanes, Aromatics, Alkenes, and Gases (N2, CO2, H2S, H2) with the PPR78 Equation of State. Industrial & Engineering Chemistry Research 52 (46), 16457-16490

[13] Rasmussen, A.F., Sandve, T.H, Bao, K., Lauser, A., Hove, J., Skaflestad, B., Klöfkorn, R., Blatt, M., Rustad, A.B., Sævareid, O., Lie, K.-A. & Thune, A. (2021). "The Open Porous Media Flow Reservoir Simulator." Computers & Mathematics with Applications, 81, 159-185 - See also: https://opm-project.org and https://github.com/OPM.

[14] Span, R., and Wagner, W. (1996). A New Equation of State for Carbon DioxideCovering the Fluid Region from the Triple-Point Temperature to 1100 K at Pressures up to 800 MPa. Journal of Physical and Chemical Reference Data. 25:1509-1596.

[15] Spycher, N., Pruess, K. 2005. CO2-H2O mixtures in the geological sequestration of CO2. II. Partitioning in chloride brines at 12-100 °C and up to 600 bar. Geochimica Cosmochimica Acta, 69 (13), 3309-3320.

[16] Spycher, N., Pruess, K., and Ennis-King, J., 2003. CO2-H2O mixtures in the geological sequestration of CO2. I. Assessment and calculation of mutual solubilities from 12 to 100°C and up to 600 bar. Geochimica Cosmochimica Acta, 67, 3015–3031.

[17] Vesovic, V., Wakeham, W.A., Olchowy, G.A., Sengers, J.V., Watson, J.T.R., and Millat, J. (1990). The Transport Properties of Carbon Dioxide. Journal of Physical and Chemical Reference Data. 19:763-80